A New Simplified Sensorless Speed Control of Induction Motor using *D*-axis Voltage

M. Tsuji*, G. M. C. Mangindaan*, Y. Kunizaki*, R. Hashimoto*, S. Hamasaki*
* Graduate School of Engineering, Nagasaki University, Japan
E-mail: mineo@nagasaki-u.ac.jp

***Abstract* —This paper presents a new simplified sensorless speed control method of induction motors (IM). The output voltage of *d*-axis PI current controller is used to compute the flux angle and to control the speed in correspondence with its reference. The effectiveness of the proposed method has been demonstrated by simulations considered PWM and experiments.**

***Index Terms*—*d*-axis voltage, root loci, speed sensorless vector control, stability**

I. INTRODUCTION

Speed sensorless vector control of IM allows high performance control of torque and speed and the system is widely used. Many model reference adaptive system (MRAS) based methods are proposed [1] - [9]. However, the configurations of the systems are relatively complicated. Because MRAS based methods need state observer and many PI controllers (*d-q* currents, speed and speed estimation).

In this paper, we present a new simplified sensorless speed control method of IM. A linear model of the proposed system is derived in state space equation by taking a small perturbation of steady state operating point. Stability analysis is performed by showing root loci of the linear model. By the stability analysis we can determine the gains of controller.

Transient response of the linear model is compared with that by nonlinear model to check if two models of proposed method are valid. The effectiveness of the proposed method has been demonstrated by simulations considered PWM and experiments.

II. PROPOSED METHOD

To simplify control scheme, we have proposed a new sensorless vector control method shown in Fig.1. [10].

The *d-q* voltage equations of the induction motor in arbitrary rotating coordinate system are described as follows:

voltage model:

$$e_{sd} = (R_s + \sigma L_s p) i_{sd} - \omega \sigma L_s i_{sq} + \frac{Mp}{L_r}\psi_{rd} - \frac{\omega M}{L_r}\psi_{rq} \quad (1)$$

$$e_{sq} = \omega \sigma L_s i_{sd} + (R_s + \sigma L_s p) i_{sq} + \frac{\omega M}{L_r}\psi_{rd} + \frac{Mp}{L_r}\psi_{rq} \quad (2)$$

current model:

$$0 = -\frac{M}{\tau_r} i_{sd} + (\frac{1}{\tau_r} + p)\psi_{rd} - (\omega - \omega_r)\psi_{rq} \quad (3)$$

$$0 = -\frac{M}{\tau_r} i_{sq} + (\omega - \omega_r)\psi_{rd} + (\frac{1}{\tau_r} + p)\psi_{rq} \quad (4)$$

In the steady state, the voltage model becomes:

$$e_{sd} = R_s i_{sd} - \omega \sigma L_s i_{sq} - \frac{\omega M}{L_r}\psi_{rq} \quad (5)$$

$$e_{sq} = \omega \sigma L_s i_{sd} + R_s i_{sq} + \frac{\omega M}{L_r}\psi_{rd} \quad (6)$$

In the proposed method, by using the output voltage of *d*-axis PI current control, we estimate the phase of rotor flux by changing it to satisfy that ψ_{rq} of (5) becomes zero. The *d*-axis PI current controller of Fig.1 is expressed as

$$e_d^* = K_P \left(i_{sd}^* - i_{sd} \right) + e_{cd} \quad (7)$$

where, $pe_{cd} = K_I \left(i_{sd}^* - i_{sd} \right)$

By using the e_d^* of Fig.1 and (5), we have following equation

$$e_d^* - R_s^* i_{sd}^* = -\omega^* M \psi_{rq} / L_r \quad (8)$$

By controlling i_{sd}^* constant, and assuming that $\psi_{rq} = 0$ in (3), we have

$$\psi_{rd} = M i_{sd}^* \quad (9)$$

By assuming that $\psi_{rq} = 0$ in (4) and using (9), slip frequency ω_e is computed as

$$\omega_e = \frac{i_{sq}}{\tau_r^* i_{sd}^*} \quad (10)$$

We estimate the flux frequency ω^* so as to bring *q*-axis flux zero by using P controller shown in Fig.1

$$\omega^* = \omega_r^* + \omega_e - K_\omega \left(e_d^* - R_s^* i_{sd}^* \right) \quad (11)$$

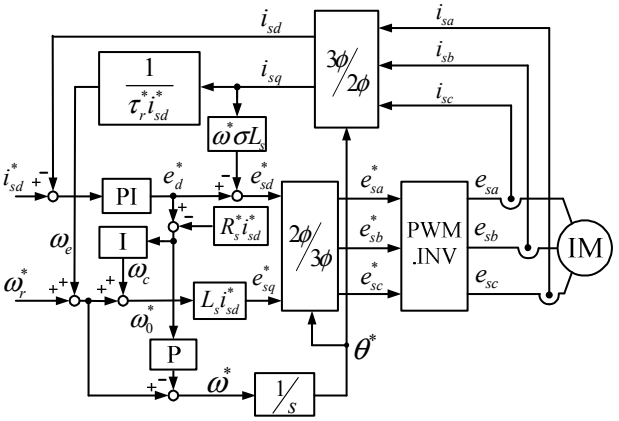

Fig.1. Block diagram of proposed method.

where, $K_\omega = sign(\omega^*)|K_\omega|$. Value of K_ω is positive if ω^* is greater than zero, and K_ω is negative if ω^* is less than zero. Slip frequency ω_e is added to speed command ω_r^*. The following integral controller computes the angular frequency ω_c that control torque and speed.

$$p\omega_c = \frac{K_\omega}{T_\omega}\left(e_d^* - R_s^* i_{sd}^*\right) \tag{12}$$

The q-axis voltage e_{sq}^* is computed by neglecting the voltage drop of stator resistance, but it is compensated by ω_c.

$$e_{sq}^* = \omega_0^* L_s i_{sd}^* \tag{13}$$

where, $\omega_0^* = \omega_r^* + \omega_e + \omega_c$.

In steady-state, ψ_{rq} must be zero by the action of integral controller, and then the following relation is valid.

$$\omega_r^* + \omega_e = \omega^* \tag{14}$$

When (14) is satisfied, the rotor speed is equal to its command. In proposed system of Fig.1, any observer is not used and d-axis PI controller and P and I frequency controllers are only used. Therefore, the proposed system is much simpler than conventional systems.

III. STABILITY ANALYSIS

Taking a small perturbation at steady-state operating point, a linear model of proposed system is derived. System stability is discussed by using root loci. A linear model of the proposed system is derived in form

$$p\Delta \boldsymbol{x} = \boldsymbol{A}\Delta \boldsymbol{x} + \boldsymbol{B}\Delta \omega_r^* + \boldsymbol{B}_L \Delta T_L \tag{15}$$

$$\Delta \boldsymbol{x} = \left[\Delta i_{sd}\ \Delta i_{sq}\ \Delta\psi_{rd}\ \Delta\psi_{rq}\ \Delta\omega_r\ \Delta e_{cd}\ \Delta\omega_c\right]^{\mathrm{T}}$$

$$a_1 = \frac{R_s}{\sigma L_s} + \frac{M^2}{\sigma L_s L_r \tau_r},\ a_2 = \frac{M\ p^2}{4JL_r}$$

$$\boldsymbol{A} = \begin{bmatrix} -a_1 - \dfrac{K_P}{\sigma L_s} & 0 & \dfrac{M}{\sigma L_s L_r \tau_r} & \dfrac{M\omega_r}{\sigma L_s L_r} & \dfrac{M\psi_{rq}}{\sigma L_s L_r} & \dfrac{1}{\sigma L_s} & 0 \\ -\omega^* - i_{sd}K_\omega K_P & -a_1 + \dfrac{1}{\sigma\tau_r^*} - \dfrac{1}{\tau_r^*} & -\dfrac{M\omega_r}{\sigma L_s L_r} & \dfrac{M}{\sigma L_s L_r \tau_r} & -\dfrac{M\psi_{rd}}{\sigma L_s L_r} & i_{sd}K_\omega & \dfrac{i_{sd}^*}{\sigma} \\ \dfrac{M}{\tau_r} + \psi_{rq}K_\omega K_P & \dfrac{\psi_{rq}}{\tau_r^* i_{sd}^*} & -\dfrac{1}{\tau_r} & \omega^* - \omega_r & -\psi_{rq} & -\psi_{rq}K_\omega & 0 \\ -\psi_{rd}K_\omega K_P & \dfrac{M}{\tau_r} - \dfrac{\psi_{rd}}{\tau_r^* i_{sd}^*} & \omega_r - \omega^* & -\dfrac{1}{\tau_r} & \psi_{rd} & \psi_{rd}K_\omega & 0 \\ -a_2\psi_{rq} & a_2\psi_{rd} & a_2 i_{sq} & -a_2 i_{sd} & 0 & 0 & 0 \\ -K_I & 0 & 0 & 0 & 0 & 0 & 0 \\ -\dfrac{K_\omega K_P}{T_\omega} & 0 & 0 & 0 & 0 & \dfrac{K_\omega}{T_\omega} & 0 \end{bmatrix}$$

$$\boldsymbol{B} = \begin{bmatrix} 0 \\ \dfrac{i_{sd}^*}{\sigma} - i_{sd} \\ \psi_{rq} \\ -\psi_{rd} \\ 0 \\ 0 \\ 0 \end{bmatrix},\ \boldsymbol{B}_L = \begin{bmatrix} 0 \\ 0 \\ 0 \\ 0 \\ -\dfrac{P}{2J} \\ 0 \\ 0 \end{bmatrix}$$

System is stable when all eigenvalues of matrix $\boldsymbol{A}$ are in the left half of the s-plane.

Fig.2 shows root loci when the slip speed N_{sl} and T_ω of I controller are changed. In Fig.2 (a), the speed command N_r^* is 700 rpm, K_ω = 3.0, T_ω varies from 0.01 to 0.05, and N_{sl} varies from -80 rpm to 80 rpm. System becomes unstable by the root near the point $j60$ especially at motoring operation when T_ω =0.01. In Fig. (b), the increase in T_ω causes instability by the root near the point $j5$ especially at regenerating operation.

Fig.3 shows root loci when the slip speed N_{sl} and the gain K_ω of P and I frequency controllers are changed. The speed command N_r^* is at 700 rpm, T_ω = 0.05, K_ω varies from 0.01 to 10.0, and N_{sl} varies from -80 rpm to 80 rpm. The value of T_ω is chosen from root loci of Fig.2 (a) as 0.05. When K_ω = 0.1 and slip speed N_{sl} is in regenerating operating points, all poles are in unstable region on positive real axis. From Fig.3, stable operations are obtained in all load condition when K_ω = 3.0 or K_ω = 10.0, then we choose that K_ω = 3.0 in experimental system.

Fig.4 shows the root loci when N_r^* is 700 rpm and N_{sl} is 35 rpm. In this figure, K_ω varies from 0.01 to 100.0 and T_ω from 0.01 to 0.10. It is observed that the small values of K_ω and T_ω result in unstable or oscillating operation.

To examine the stability at low speed operation and at higher speed one, root loci at 100 rpm and 1500 rpm are computed for selected parameter.

In Fig.5, the root loci are shown when T_ω = 0.05, K_ω = 3.0, and N_r^* = 100 rpm for the change of slip speed N_{sl}. The system can work in stable region in motoring and regenerating operation.

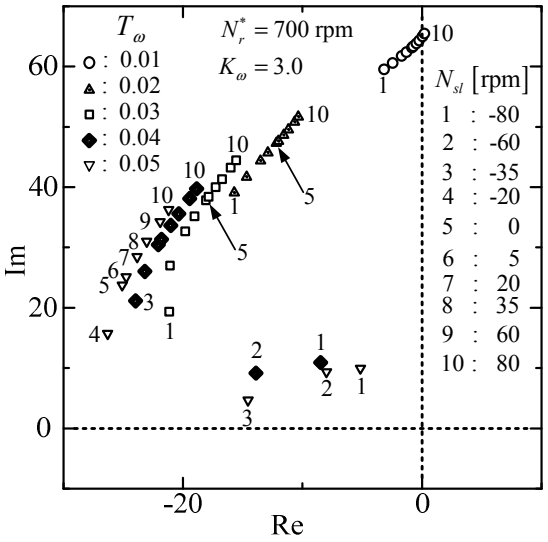

(a) $T_\omega : 0.01 - 0.05$.

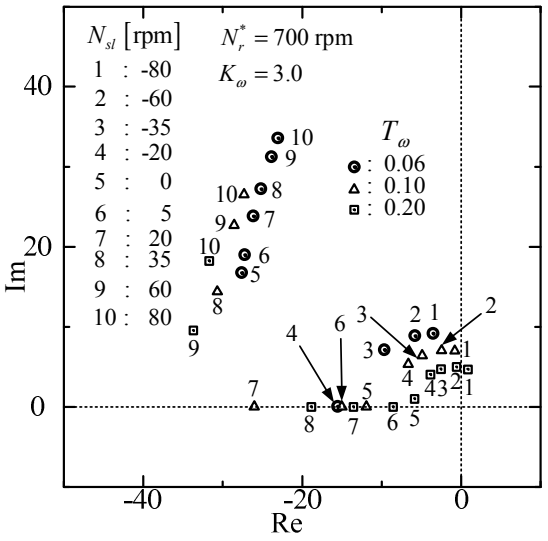

(b) $T_\omega : 0.06 - 0.10$.

Fig.2. Root loci with parameters T_ω and N_{sl}.

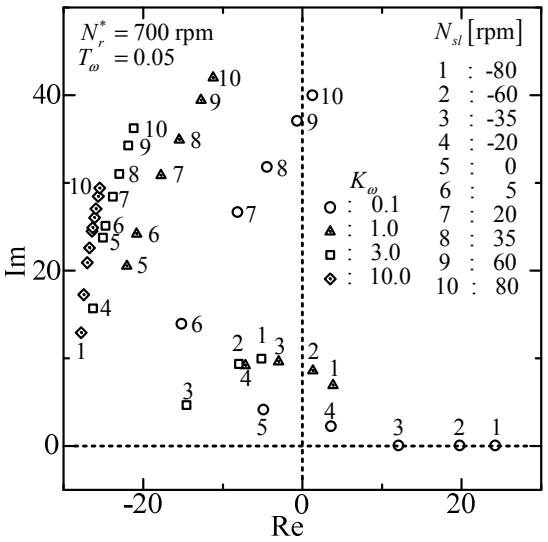

Fig.3. Root loci with parameters K_ω and N_{sl}.

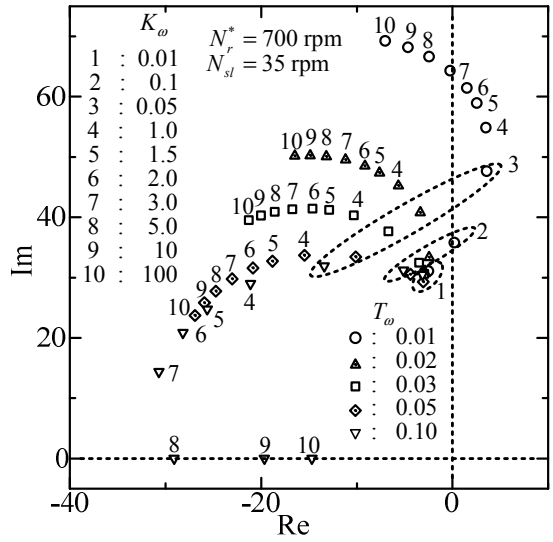

Fig.4. Root loci with parameters T_ω and K_ω.

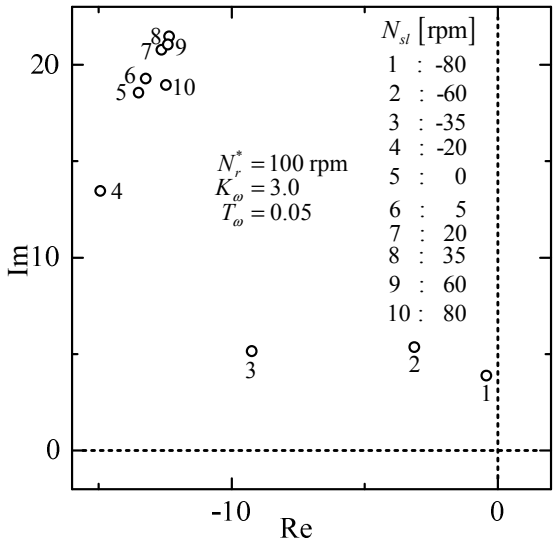

Fig.5. Root loci at $N_r^* = 100$ rpm.

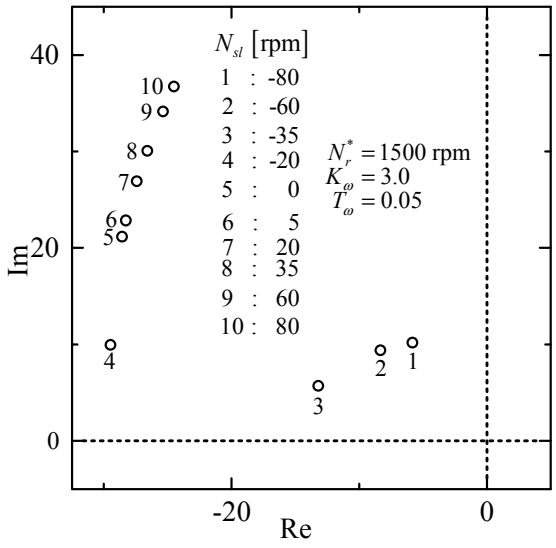

Fig.6. Root loci at $N_r^* = 1500$ rpm.

In Fig.6, the root loci are shown when T_ω = 0.05, K_ω = 3.0, and N_r^* = 1500 rpm. The system is stable in all operating points.

Comparison between Fig.5 and Fig.6 shows that the system works more stable at higher speeds both motoring and regenerating operation because with increasing speed, the roots have smaller real part.

Fig.7 shows the transient responses for the step change of speed command from 700 rpm to 710 rpm and back to 700 rpm. The load torque T_L is 4 Nm, T_ω = 0.05 and K_ω = 0.5.

The result of linear model (15) is shown in Fig. (a), and nonlinear model result is shown in Fig. (b). The nonlinear model uses the equations which are obtained when the linear model is derived. The results of the linear model are close to those of the nonlinear model. It is confirmed that the derivation of the linear model (15) is correct.

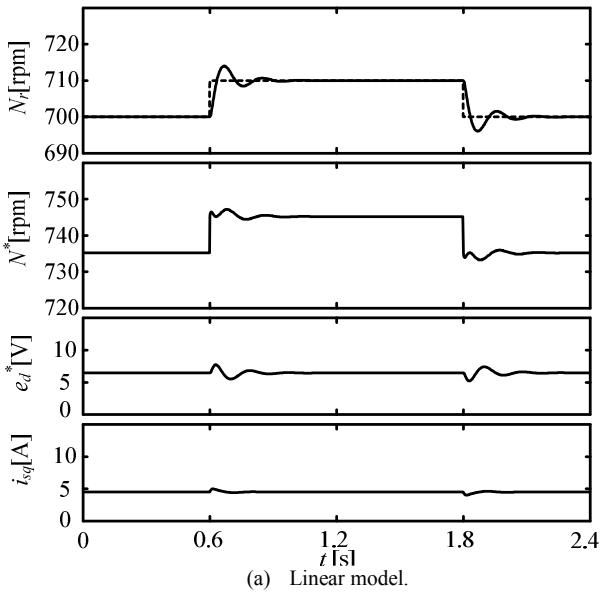

(a) Linear model.

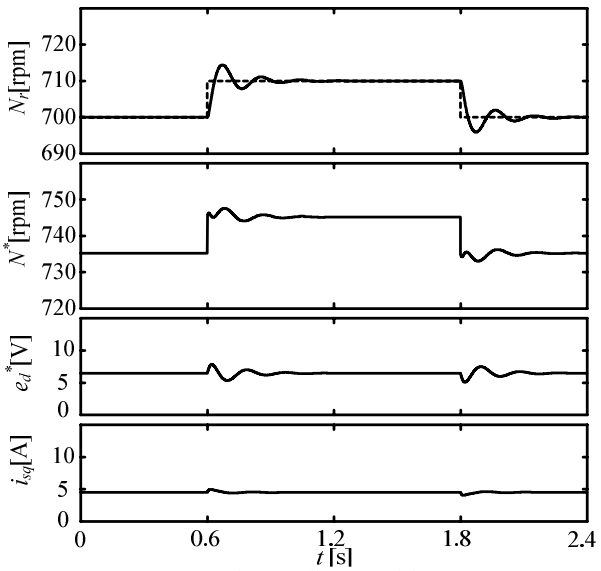

(b) Nonlinear model.

(700 →710 →700 rpm, T_L=4 N-m, K_ω = 0.5, T_ω= 0.05).

Fig.7. Transient responses for the step change of speed command.

IV. Experimental and Simulation Results

The proposed control system is implemented by a DSP (TMS320C32)-based PWM inverter as shown in Fig.8. Sampling period used in this system is 200 μs. Because the dead time and the non-ideal features of IGBT influence the output voltage of the inverter, a compensating algorithm is developed for the experimental system [8]. Parameters of IM are: number of pole P=4, stator resistant R_s =1.54Ω, rotor resistant R_r=0.787Ω, stator and rotor inductance L_s=L_r=0.0115H, mutual inductance M=0.11H, and moment of inertia J=0.0126 kgm^2.

In Figs.9 – 11, the speed command is changed from 700 rpm to 800 rpm and then 700 rpm in the monitoring operation at load torque of 4 N-m for three different values of K_ω.

When K_ω = 3.0, the transient response is shown in Fig.9. The nonlinear simulation result of (a) is obtained by considering PWM switching in detail. Because of the PWM switching, high frequency ripples are observed in the waveforms of the synchronous speed N^* , d-axis voltage e_d^* and q-axis current i_{sq} . Experimental results of (b) are similar to those of nonlinear simulation. On the other hand, the results of linear model (15) do not contain high frequency ripples as shown in Fig.(c). However, the low frequency responses are similar to those of Figs.(a) and (b).

Fig.10 gives the results when K_ω = 0.5. By comparing the results of Fig.10 with those of Fig.9, it is observed that the oscillation is increased and the settling time of actual speed to speed command becomes longer, and the overshoot of speed is larger. Good correlation between the nonlinear simulation result and experimental one is also obtained. However, the result of linear model has slightly moderate response because of nonlinear characteristic.

Fig.11 gives the results when K_ω = 5.0. By comparing Fig.9 and Fig.11, the ripple of N^* in Fig.11 becomes larger in the nonlinear simulation and experimental result. In experimental result, the effect of noise is expanded by large gain of K_ω in Fig.11 (b). However, the actual speed smoothly converges to the speed command and the results of actual speed in all cases are almost same.

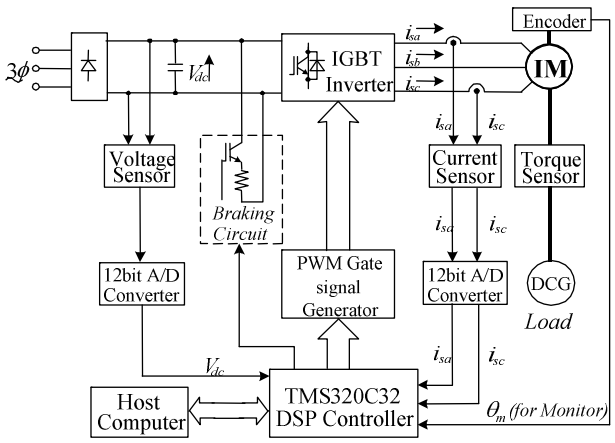

Fig.8. Experimental system.

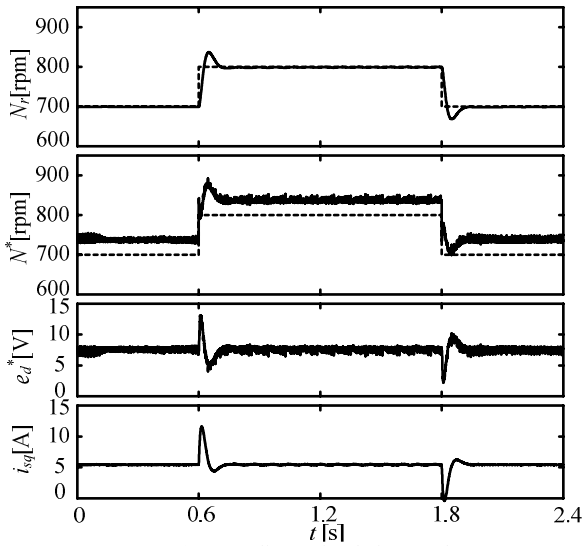

(a) Nonlinear simulation result.

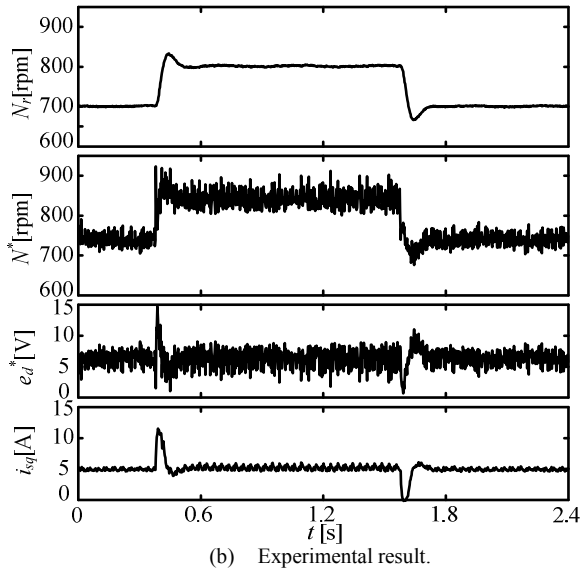

(b) Experimental result.

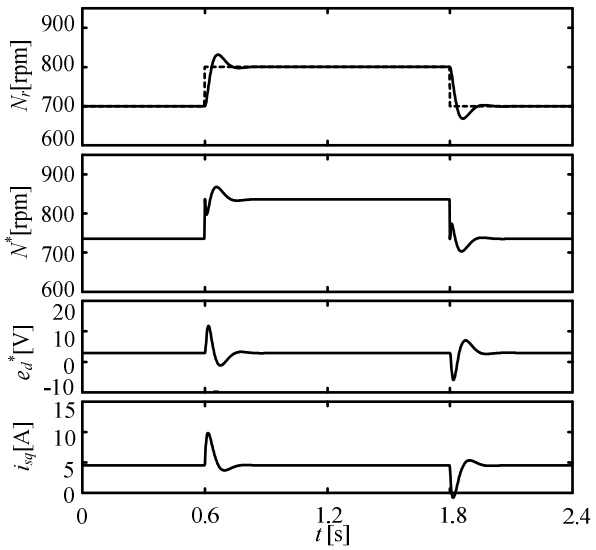

(c) Linear model result.

(700 → 800 → 700 rpm , T_L=4 N-m, K_ω = 3.0, T_ω= 0.05).

Fig.9. Responses for the step change of speed command.

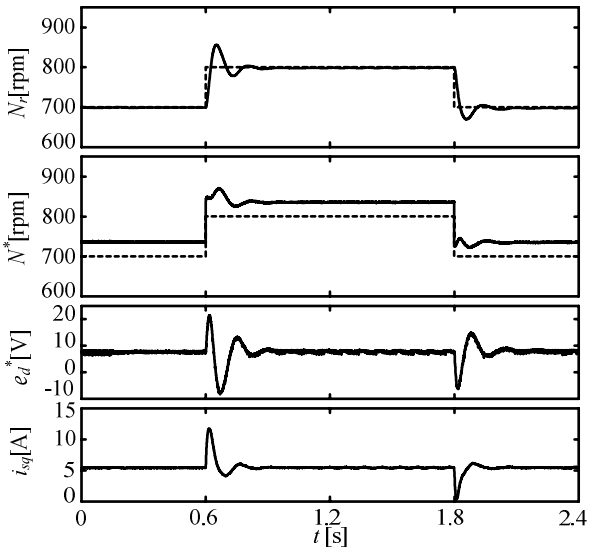

(a) Nonlinear simulation result.

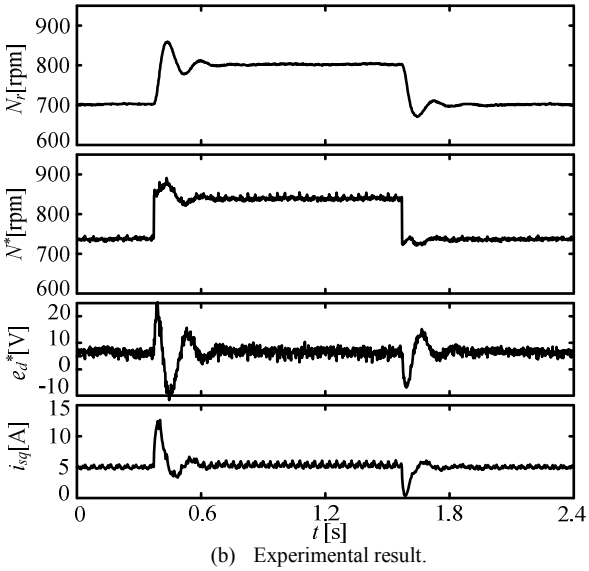

(b) Experimental result.

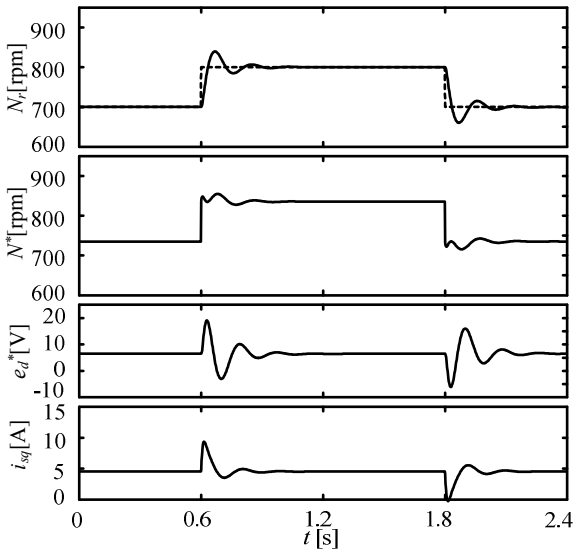

(c) Linear model result.

(700 → 800 → 700 rpm, T_L = 4 N-m, K_ω = 0.5, T_ω= 0.05).

Fig.10. Responses for the step change of speed command.

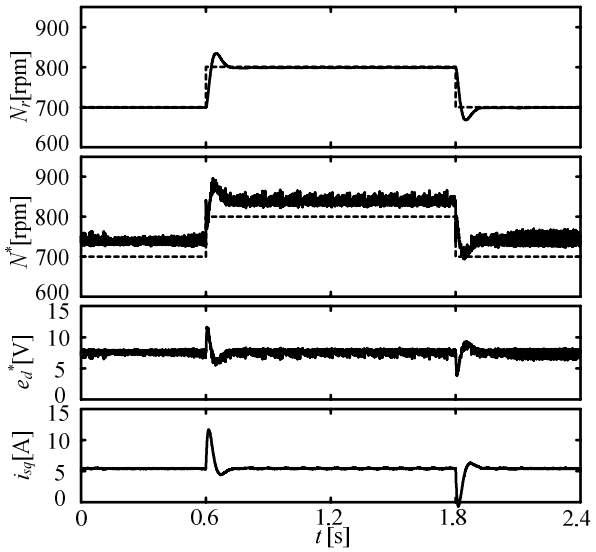

(a) Nonlinear simulation result.

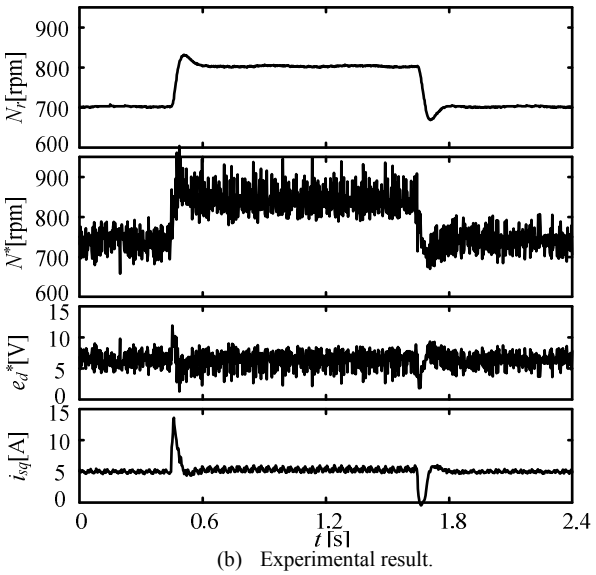

(b) Experimental result.

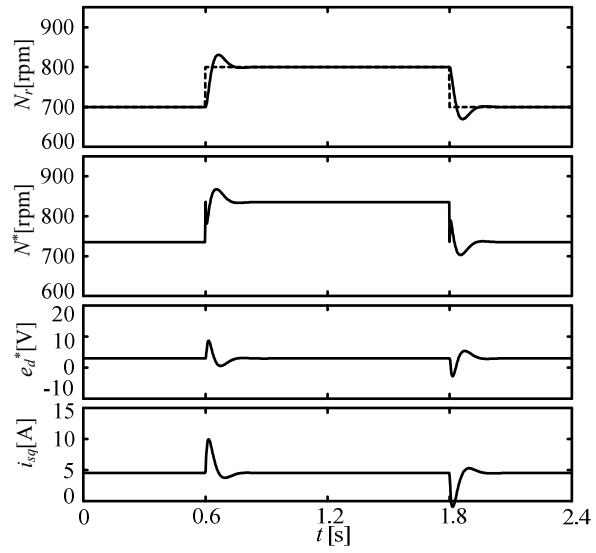

(c) Linear model result.
(700 → 800 → 700 rpm, T_L = 4 N-m, K_ω = 5.0, T_ω = 0.05).
Fig.11. Responses for the step change of speed.

V. CONCLUSIONS

The conclusions drawn from this study are summarized as follows:

(1) We have proposed a new simplified sensorless vector control method of IM.
(2) P control for flux angle computation and I control for torque and speed are realized by using the output voltage of *d*-axis PI controller.
(3) A linear model is derived and the root loci are used to design the control parameters.
(4) It is demonstrated that the proposed system can realize stable operation in both motoring and regenerating modes by the result root loci.
(5) The experimental results agree with those of nonlinear simulation and the usefulness of proposed method is verified.

REFERENCES

[1] C. Schauder, "Adaptive speed identification for vector control of induction motors without rotational transducers", *IEEE Trans. Industr. Applic.*, Vol.28, No.5, pp. 1054-1061, Sep./Oct. 1992.

[2] H. Tajima, Y. Hori, "Speed sensorless field orientation control of the induction machine." *IEEE IAS Annual Meeting*, pp. 385-391, 1991.

[3] H. Kubota, K. Matsuse, "Speed sensorless field oriented control of induction machines using flux observer", *IEEE IECON*, pp. 1611-1615, 1994.

[4] K. Matsuse, T. Yoshizumi, S. Katsuta, and S. Taniguchi, "High-response flux control of direct field-oriented induction motor with high efficiency taking core loss into account", *IEEE Trans. Industr. Applic.*, Vol.35, No.1, pp. 62-69, Jan./Feb. 1999.

[5] H. Sugimoto, L. Ding, "A consideration about stability of vector controlled induction motor systems using adaptive secondary flux observer", *Trans. IEEJapan*, Vol.119-D, No.10, pp.1212-1222, 1999.

[6] M. Tursini, R. Petrella, and F. Parasiliti, "Adaptive sliding mode observer for speed sensorless control of induction motors", *IEEE Trans. Industr. Applic.*, Vol.36, No.5, pp.1380-1387, Sep./Oct. 2000.

[7] Y. Kinpara, M. Koyama, "Speed sensorless vector control method of induction motor including a low speed region", *Trans. IEEJapan*, Vol.120-D, No.2, pp.223-229, 2000.

[8] M. Tsuji, S. Chen, K. Izumi and E. Yamada, "A sensorless vector control system for induction motors using q-axis flux with stator resistance identification", *IEEE Trans. Industrial Electronics*, Vol.48, No.1, pp. 185-194, February 2001.

[9] M. Hinkkanen, "Analysis design of full-order flux observers for sensorless induction motors", *IEEE Trans. Industrial Electronics*, Vol.51, No.5, pp. 1033-1040, October 2004.

[10] M. Tsuji, R. Hashimoto, S. Hamasaki, "A simple speed sensorless vector control of induction motor using *q*-axis flux", *The Papers of Technical Meeting IEEJapan*, RM-11-130, pp.31-36, 2011.